A Spectral Integral Method and Hybrid SIM/FEM for Layered Media

Ergün Şimşek, *Student Member, IEEE*, Jianguo Liu, *Student Member, IEEE*, and Qing Huo Liu, *Fellow, IEEE*

***Abstract*—This paper first presents a spectral integral method (SIM) for electromagnetic scattering from homogeneous dielectric and perfectly electric conducting objects straddling several layers of a multilayered medium. It then uses this SIM as an exact radiation boundary condition to truncate the computational domain in the finite-element method (FEM) to form a hybrid SIM/FEM, which is applicable to arbitrary inhomogeneous objects. Due to the high accuracy of the SIM, the sampling density on the radiation boundary requires less than five points per wavelength to achieve 1% accuracy. The efficiency and accuracy of the developed methods have been demonstrated with several numerical experiments for the TM_z case. The TE_z case can be obtained by duality.**

***Index Terms*—Boundary-element method (BEM), finite-element method (FEM), layered media, radiation boundary condition (RBC), spectral integral method (SIM), surface integral equation (SIE).**

I. Introduction

ELECTROMAGNETIC scattering from inhomogeneous objects of arbitrary shape embedded in a layered medium has been a very important research topic because of its wide application in areas such as geophysical exploration, remote sensing, landmine detection, biomedical imaging, interconnect simulations, microstrip antennas, and monolithic microwave integrated circuits. The complex background and the large number of unknowns associated with realistic targets make the problem more challenging.

For homogeneous objects embedded in a layered medium, surface integral equations (SIEs) are more appropriate than volume integral equations (VIEs). However, for inhomogeneous objects, the SIE must be combined with other methods such as the finite-element method (FEM) in order to account for the inhomogeneity. In this approach, the computational domain can be truncated by using a radiation boundary condition (RBC). Over the last three decades, several RBCs have been developed [1]–[21]. One of them is the hybrid finite-element method/boundary-element method (FEM/BEM), which uses the SIE as an RBC on the boundary surrounding the scatterer(s), and the FEM in the bounded region [2]–[6], [11], [13]. In this approach, the evaluation of the layered-medium Green's functions is a time-consuming step of the overall procedure, which is $O(N_b^2)$, where N_b is the number of the samples taken on the boundary. The classical methods such as the method of moments (MoM) requires at least ten points per wavelength sampling density to achieve 1% accuracy. If one can reduce this requirement to the half: 1) this time-consuming step takes only a quarter of the classical approach and 2) the matrix size of the problem is reduced. Fortunately, the number of the required samples taken on the boundary can be decreased depending on the accuracy of the SIE. Due to this lower memory requirement and geometrical and material adaptability, the FEM/BEM is a useful and powerful method for analysis of scattering by inhomogeneous objects in layered media.

The matrix size of the FEM problem depends on the accuracy of the basis functions used for both the FEM and BEM. Most of the published results use zeroth- and first-order basis functions, thus requiring at least ten points per wavelength sampling density in the discretization. The usage of higher order methods can reduce the minimum required sampling density.

A spectral integral method (SIM), which has been developed to solve the SIE for electromagnetic scattering by homogeneous objects with a smooth boundary in a homogeneous background [22] and in layered media [23] is an efficient higher order method. The usage of the fast Fourier transform (FFT) algorithm provides exponentially accurate results, and it has been shown that approximately three points per wavelength guarantees an error less than 1%. As a result, using this exponentially accurate method, i.e., SIM, as an RBC can reduce the minimum required sampling density on the radiation boundary. Recently, Liu and Liu propose that the SIM can be utilized as an efficient RBC to truncate the computational domain in the FEM for a homogeneous background medium [24].

This study is the extension of the SIM/FEM to layered-medium problems. It has two new contributions: first, it extends the SIM for objects completely embedded in a single layer, as described in [23], to objects straddling several layers. To achieve this, we improve the SIM to handle the fields and Green's function across the layer interfaces so that SIM can now be applied to a scatterer straddling several layers. This new feature is nontrivial and greatly expands the applicability of the SIM. Secondly, the SIM is used as an RBC for the FEM in layered-medium problems. This allows the objects inside the surface to be arbitrarily inhomogeneous. The high-order accuracy of the SIM greatly reduces the number of unknowns on the boundary integral and, hence, greatly reduces CPU time used for the evaluation of the layered-medium Green's functions.

This paper is organized as follows. In Section II, the improved SIM for objects straddling several layers is described.

Manuscript received January 1, 2006; revised May 6, 2006. This work was supported by the National Science Foundation under Grant CCR-00-98140 and Grant IIS-0086075.

The authors are with the Department of Electrical and Computer Engineering, Duke University, Durham, NC 27708-0291 USA (e-mail: qhliu@ee.duke.edu).

Color versions of Figs. 2–6 and 11 are available online at http://ieeexplore.ieee.org.

Digital Object Identifier 10.1109/TMTT.2006.883647

Section III presents the hybrid SIM/FEM for arbitrarily inhomogeneous objects in a layered medium. The SIM and SIM/FEM are validated with several numerical examples in Section IV.

II. SIM for a Homogeneous Scatterer Straddling Several Layers

Consider a general multilayered medium consisting of N layers separated by $N-1$ interfaces parallel to the x-axis. Layer $i(i=1,\ldots,N)$ exists between $y=y_i$ and y_{i-1} ($y_0\to-\infty$ and $y_N\to\infty$) and is characterized by relative complex permittivity $\tilde{\epsilon}_{r,i}$ and relative permeability $\mu_{r,i}$; the wavenumber inside the layer is given by $k_i=\omega\sqrt{\tilde{\epsilon}_i\mu_i}$. Assume that the scatterer is a homogeneous object residing in several layers of the background. The boundary of the scatterer is described as $r=r(\theta)$ or, equivalently, $[x=x(\theta), y=y(\theta)]$ in terms of a parameter θ (in this case, the azimuthal angle $\theta\in[0,2\pi]$). An incident TM_z wave is assumed and the time dependence of $e^{j\omega t}$ is implied.

For the TM_z case, the two-dimensional (2-D) Helmholtz equation for the scalar field E_z is

$$\nabla\cdot\mu_{r,\gamma}^{-1}\nabla E_z+k_0^2\tilde{\epsilon}_{r,\gamma}E_z=-f_\gamma \tag{1}$$

where subscript γ indicates the region outside ($\gamma=l$) or inside ($\gamma=d$) the object, f_γ is the source excitation, $k_\gamma=\omega\sqrt{\mu_\gamma\tilde{\epsilon}_\gamma}$, and $k_0=\omega\sqrt{\mu_0\epsilon_0}$.

For a smooth dielectric object embedded in a layered medium, one boundary integral equation on the outside of surface of the scatterer D can be obtained as

$$E_z^{\mathrm{inc}}(\mathbf{r})+\oint_D\left[\frac{\partial E_z(\mathbf{r}')}{\partial n'}G_l(\mathbf{r},\mathbf{r}')-E_z(\mathbf{r}')\frac{\partial G_l(\mathbf{r},\mathbf{r}')}{\partial n'}\right]ds'=\frac{E_z(\mathbf{r})}{2} \tag{2}$$

for $\mathbf{r}\in D$, where f_d is assumed zero, E_z^{inc} is the incident wave from outside the object (i.e., $f_l\neq0, f_d=0$), $\hat{\mathbf{n}}$ is the outward unit normal, and $G_l(\mathbf{r},\mathbf{r}')$ is the layered-medium Green's function given by

$$G_l(\mathbf{r},\mathbf{r}')=\frac{1}{\pi}\int_0^\infty\tilde{G}(k_x,y\,|\,y')\cos k_x(x-x')dk_x \tag{3}$$

where $\tilde{G}$ is the spectral-domain counterpart. $G_l(\mathbf{r},\mathbf{r}')$ can be written as

$$G_l(\mathbf{r},\mathbf{r}')=\frac{1}{\pi}\int_0^\infty\left[\tilde{G}(k_x,y\,|\,y')-\tilde{G}_{\mathrm{sub}}(k_x,y\,|\,y')+\tilde{G}_{\mathrm{sub}}(k_x,y\,|\,y')\right]\cos k_x(x-x')dk_x \tag{4}$$

where

$$\tilde{G}_{\mathrm{sub}}(k_x,y\,|\,y')=\frac{\mu_{r,m}}{2jk_{x,m}}e^{-jk_{x,m}|y-y'|} \tag{5}$$

and $\mu_{r,m}$ is the mth layer's relative permeability where the field point is and $k_{x,m}^2=k_m^2-k_x^2$. Finally, (3) can be written as

$$G_l(\mathbf{r},\mathbf{r}')=\frac{1}{\pi}\int_0^\infty\left[\tilde{G}(k_x,y\,|\,y')-\tilde{G}_{\mathrm{sub}}(k_x,y\,|\,y')\right]\times\cos k_x(x-x')dk_x+\frac{\mu_{r,m}}{4j}H_0^{(2)}(k\rho) \tag{6}$$

where $\rho=\sqrt{(x-x'^2)+(y-y')^2}$, and $H_0^{(2)}$ is the zeroth-order Hankel function of the second kind. This formulation is the same as the primary field term subtraction when source and field points are in the same layer [23], [25]–[28]. The important caution is that this subtraction procedure is used even if the source and field points are in different layers. Hence, we can separate the layered media Green's function into two parts: singular and nonsingular. As described in [29], we can define an infinitely smooth function to handle the singular behavior in terms of θ as follows:

$$\hat{G}_l(\theta,\theta')\equiv G_l(\theta,\theta')+\frac{1}{2\pi}\ln\left|2\sin\left(\frac{\theta-\theta'}{2}\right)\right|J_0(k_{l,m}R). \tag{7}$$

Similar procedure follows for the derivative of the Green's function $\partial G_l(\mathbf{r},\mathbf{r}')/\partial n'$, as described in [23], not only for the primary field term, but also for reflection terms.

The unknown field and its derivative can be approximated by truncated Fourier series in terms of θ along the boundary of the scatterer. The two integrations in (2) can then be calculated using the FFT with high accuracy. After collocation at $\{\theta_m\}$ points, (2) can be written in a compact form as follows:

$$L\tilde{\mathbf{e}}_z^b+M\tilde{\mathbf{h}}_t^b=\mathbf{E}_z^{\mathrm{inc}} \tag{8}$$

where $\tilde{e}_{zn}^b$ and $\tilde{h}_{tn}^b$ are the Fourier's coefficients of $E_z(\theta')$ and $(\partial E_z(\theta')/\partial n')$, respectively, N_s is the number of discretized Fourier transform points, $L_{mn}=e^{jn\theta_m}/2+2\pi h_{mn}+k_b v_{mn}$ and $M_{mn}=-2\pi g_{mn}+u_{mn}$, in which $m,n=1,2,\ldots,N_s$, are the indices of basis and testing points on the discrete boundary, g_{mn} and h_{mn} are Fourier transforms of the smooth parts, and u_{mn} and v_{mn} are Fourier transforms of the two nonsmooth terms of the Green's function and its normal derivative (see [23] for the expressions). Due to the use of singularity subtraction and the FFT, the calculations of these terms are convergent, fast, and have high accuracy.

The second boundary integral equation for the interior problem can be discretized in the same way. The final form of the equations can be solved for the scalar field (E_z) and its normal derivative ($\partial E_z/\partial n'$) on the boundary of the scatter. From the solution of these field variables on the boundary, the fields everywhere can be obtained by the Green's theorem.

To sum up, the SIM formulation presented in [23] is developed in such a way that now it can solve scattering problems for homogeneous objects residing in several layers of the layered medium. As mentioned above, the subtraction method described in [28] has been implemented by using the layer parameters where the field point is located even when the source point is not in that same layer. The SIM has a spectral accuracy for smooth homogeneous objects. For objects with corners, the method is still valid, but the expected accuracy decreases from smooth objects. In order to simulate inhomogeneous objects, we next develop a hybrid method combining the SIM with the FEM.

III. Hybrid SIM/FEM for Layered Media

Consider arbitrary 2-D inhomogeneous objects in a layered medium, as shown in Fig. 1. To solve the electromagnetic wave

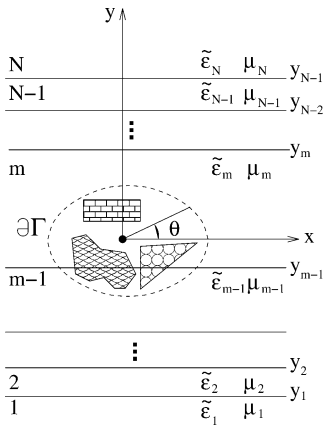

Fig. 1. Arbitrary inhomogeneous objects in an N-layer medium where each layer is characterized by relative complex permittivity $\bar{\epsilon}_{r,i}$ and relative permeability $\mu_{r,i}$. $\partial\Gamma$ is a smooth boundary containing all the scatterers.

scattering problem using the FEM, an RBC is required to truncate the computational domain so that the FEM is used in the interior region (Region I) without having to discretize the layered medium. With a correct RBC on the surface $\partial\Gamma$, the field in the layered medium, the exterior region (Region II) can be calculated once the field in Region I (including the boundary) is solved. In Region I, the material is inhomogeneous with relative permeability $\mu_r(x,y)$ and complex relative permittivity $\tilde{\epsilon}_r(x,y)$. There may also exist metallic materials and electric/magnetic sources in Region I. Region II is a layered medium described in Section II. The goal is to solve for the electromagnetic fields scattered by the inhomogeneous object.

For TM_z waves, the total electric field $E_z(x,y)$ in Region I (bounded by $\partial\Gamma$) can be determined from the solution of the scalar wave equation (1). To discretize (1), we multiply the equation by the testing function, and integrate over Region I. For the FEM solution, Region I is discretized into triangular elements and linear pyramid basis functions are used to expand the electric field $E_z(x,y)$ in the interior Region I, and triangular basis functions are used to expand the boundary value $(\partial E_z/\partial n)$ on $\partial\Gamma$ (with nodal points collocated with the nodal points of the pyramid basis function on the boundary).

Additional conditions are provided by the RBC. In order to use the SIM as an RBC for the FEM, we need to relate the electric field and its normal derivative on the boundary $\partial\Gamma$. Since $\tilde{e}^b_{zn}$ and $\tilde{h}^b_{tn}$ are the Fourier coefficients of the electric field and its normal derivative on the boundary, the pyramid basis expansion coefficients e^b_{zm} and h^b_{tm} can be obtained by $\tilde{e}^b_{zn}$ and $\tilde{h}^b_{tn}$, which are obtained from (8) through trigonometric interpolation

$$e^b_{zm} = \frac{1}{N_s}\sum_{n=-N_s/2}^{N_s/2-1} e^{jn(\theta^F_m-\theta_1)}\tilde{e}^b_{zn} \tag{9}$$

$$h^b_{tm} = \frac{1}{N_s}\sum_{n=-N_s/2}^{N_s/2-1} e^{jn(\theta^F_m-\theta_1)}\tilde{h}^b_{tn} \tag{10}$$

where $\{\theta^F_m\}$ are the positions of the FEM nodal points on the boundary in terms of the parameter θ, and θ_1 is the first discretization point for the SIM. Finally, we obtain the following system of equations (see [24] for the details):

$$Z^i\mathbf{e}^i_z + X^T_b T\tilde{\mathbf{e}}^b_z = \mathbf{S} \tag{11}$$

$$X_b\mathbf{e}^i_z + Z^b T\tilde{\mathbf{e}}^b_z + KT\tilde{\mathbf{h}}^b_t = 0. \tag{12}$$

Combining (11) and (12) with (8), one can solve the linear equations for $\tilde{e}^b_{zn}, \tilde{h}^b_{tn}$ and e^i_{zn}, thus obtaining the electric field in Region I. Using the inverse FFT, the electric field E_z and its normal derivative $\nabla E_z\cdot\hat{n}$ are obtained on the boundary $\partial\Gamma$.

Due to the high accuracy of SIM and trigonometric interpolation operations, even a small sampling density of approximately five points per wavelength (5 PPWs) can give an accuracy better than 1%. On the other hand, the FEM used for the interior region has a second-order accuracy; thus, the overall accuracy of the hybrid SIM/FEM will depend on the accuracy of the FEM part. In fact, in all the calculations, we choose N_s much smaller than N_b to accomplish SIM and trigonometric interpolation with the same accuracy as the FEM. The system in (8), (11), and (12) and is overdetermined because we have $N_i+N_b+N_s$ equations and N_i+2N_s unknowns, therefore, an iterative solver would be preferred to solve this system. Alternatively, multiplying (12) by T^+, the conjugate transpose of the trigonometric interpolation matrix T, the system matrix becomes square and, thus, a direct solver can also be used.

The advantage of the hybrid SIM/FEM method is the highly accurate RBC with very few discretization points on the boundary. Indeed, the number of unknowns in the original FEM is N_i+2N_b points (N_i+N_b) points for the electric field, and N_b points for the normal derivative of the electric field on the boundary), the SIM/FEM hybrid method has N_i+2N_s unknowns, where the ratio of $N_b/N_s>2$ as the sampling density in FEM and SIM is approximately ten points per wavelength (or more) and 5 PPWs for roughly 1% accuracy. Therefore, the number of unknowns in the SIM/FEM hybrid method is actually smaller than the FEM with a Neumann boundary condition. Furthermore, the time-consuming step of the overall method, which is the evaluation of the layered media Green's functions, is reduced by a factor of 4 (for $N_b/N_s=2$), which is a crucial reduction in terms of CPU time. In Section IV, we will show the numerical results of the hybrid SIM/FEM method.

IV. Numerical Results

For all the examples presented here, the scatterer is excited with TM_z plane wave incident normally to the interface ($\theta^{\mathrm{inc}}=90^\circ$). The TE_z case can be easily obtained by using duality. In the figures describing the geometry of the example, an artificial radiation boundary $\partial\Gamma$, which is placed at least one element away from the scatterers, is plotted with a dashed line enclosing all the scatterers.

A. Numerical Example for the SIM

First we present an example to show the validity of the SIM for a homogeneous object straddling a layer interface. A circular perfect electric conductor (PEC) cylinder with radius $r=0.25\lambda_1=12.5$ cm is partially buried in a two-layer medium, as shown in Fig. 2(a). The frequency of the incident wave is 300 MHz; the two layers have properties

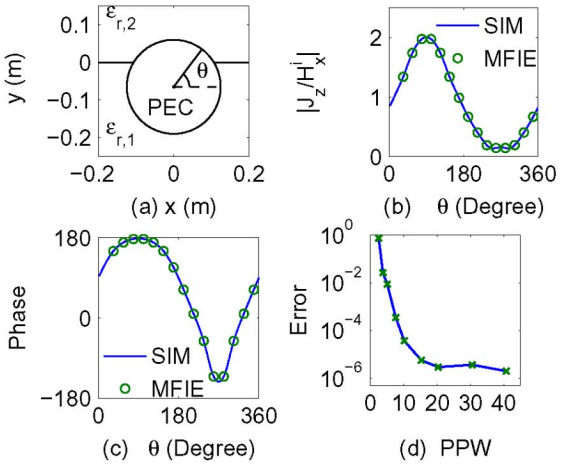

Fig. 2. (a) Partially buried PEC cylinder of radius $r = 12.5$ cm, whose center is 6.5 cm below the interface. $\mu_{r,2} = \epsilon_{r,2} = \mu_{r,1} = 1, \epsilon_{r,1} = 4, f = 300$ MHz. (b) Magnitude of current induced on the object. (c) Phase of current (in degree). (d) Convergence of error with the number of discretization points on the surface of the scatterer.

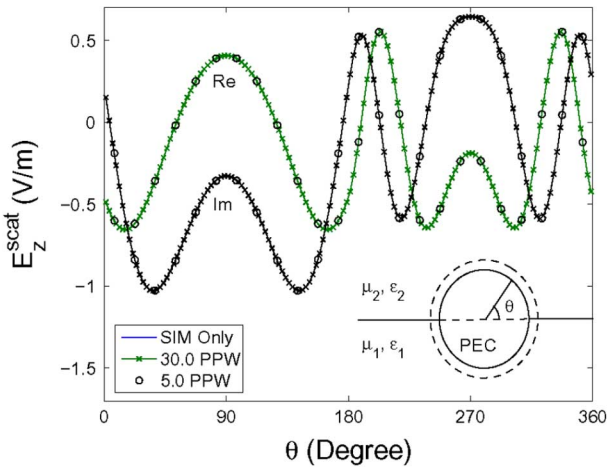

Fig. 3. Scattered field along the radiation boundary ($r_{\text{bound}} = 0.6$ m) for a circular PEC object centered on the interface of a two-layer medium. $r_{\text{pec}} = 0.5$ m, $\mu_{r,2} = \epsilon_{r,2} = \mu_{r,1} = 1, \epsilon_{r,1} = 4, f = 300$ MHz.

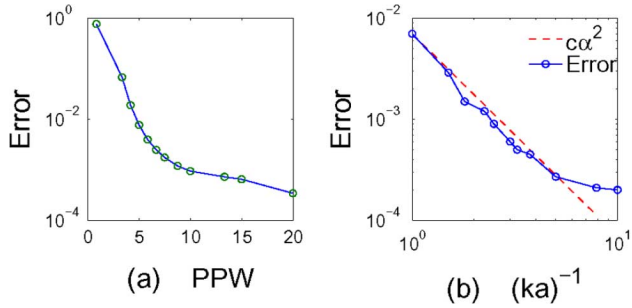

Fig. 4. Convergence of error for *Example A*: (a) with the number of discretization points along the radiation boundary and (b) with decreasing frequency.

$\mu_{r,2} = \epsilon_{r,2} = 1, \mu_{r,1} = 1, \epsilon_{r,1} = 4$. The center of the object is 6.5 cm below the interface.

Fig. 2(b) and (c) compares the magnitude and phase of the current induced on the scatterer obtained with the SIM and magnetic-field integral-equation (MFIE) formulation [30]. There is a very good agreement between these two results. The convergence of error with the number of discretization points per wavelength is obtained by using the case with 82 PPWs as a reference and is plotted in Fig. 2(d). The error decreases exponentially with the number of discretization points, confirming that the SIM has a spectral accuracy. The result shows that even with a small discretization number $N = 8$ (or at 5.0 PPWs) on the boundary of the cylinder, the relative error is smaller than 1%. Note that the Green's functions for the background have been calculated with 10^{-7} relative error tolerance, and the minimum relative error that can be obtained is approximately on this level.

B. Circular Cylinder/Circular Boundary by SIM/FEM

Next, a circular PEC object with radius of 0.5 m is centered on the interface of a two-layer medium. The top layer is air $(\epsilon_{r,2} = \mu_{r,2} = 1)$ and the bottom layer is soil $(\epsilon_{r,1} = 4, \mu_{r,1} = 1)$. The frequency is 300 MHz and the radiation boundary is a circle with radius of 0.6 m. To apply the FEM in the interior region, the interior domain is discretized into triangular elements using NETGEN (NETGEN/NGSolve V4.4, developed at Johannes Kepler University, Linz, Austria). The number of triangular elements is 2102, and the number of FEM nodes is 1257. Fig. 3 shows the scattered field along the radiation boundary obtained in two different ways. First, the SIM (30 PPWs) is used to solve the problem for $(\partial E_z(\theta')/\partial n')$ on the surface of the scatterer, and then the scattered field is calculated by using the SIE. Second, the SIM (30 PPWs) is used as an RBC on the radiation boundary, and the FEM is used for the interior region, as explained. An excellent agreement has been observed between these results. In the same figure, the result that is obtained by using 5 PPWs only is also depicted, which has very good agreement with others.

The convergence of the SIM/FEM method is analyzed in two different ways. First, as shown in Fig. 4(a), the number of SIM points on the radiation boundary is changed for the fixed frequency and sampling density for the interior region. Clearly, 5 PPWs guarantees 1% accuracy. Second, the frequency of the problem is changed for the same mesh, the number of the SIM points is 36 (4.77 PPWs for $f = 300$ MHz). Fig. 4(b) shows the convergence of error with decreasing frequency. Note that this result shows an overall second-order convergence because of using linear basis and testing functions in the FEM part.

Note that there are 224 FEM boundary nodes in this example, which is 6.2 times the number of SIM boundary nodes. The layered-medium Green's function calculation took a 38.7 times less amount of time then an FEM with a Neumann boundary condition implementation. Moreover, in the SIM/FEM method, the total number of unknowns is $N_i + 2N_s = 1105$; by contrast, for an FEM with a Neumann boundary condition, the number of unknowns would have been $N_i + N_b = 1257$, which is still greater than the number of unknowns in the SIM/FEM method. To further reduce the number of unknowns in the SIM/FEM method, in the future one can ideally combine the SIM with a higher order FEM to improve the efficiency of the overall scheme.

We have also modeled a circular PEC object with radius of 0.125 m (same as [30]), which is four times smaller than the above presented example, and the SIM results agree well with [26] and [30], but are not shown here for brevity.

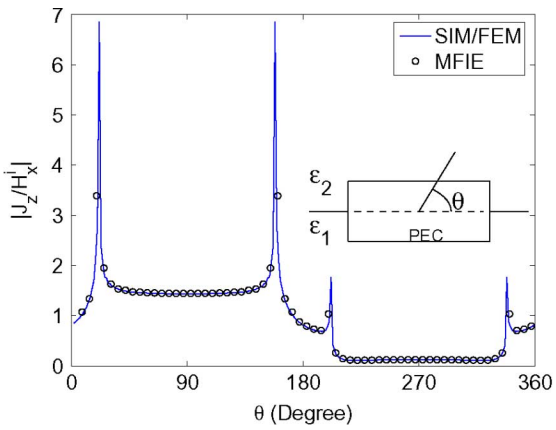

Fig. 5. Normalized magnitude of current induced on a half buried rectangular PEC object (12.5 cm × 5 cm). $\mu_{r,2} = \epsilon_{r,2} = \mu_{r,1} = 1, \epsilon_{r,1} = 4, f = 300$ MHz.

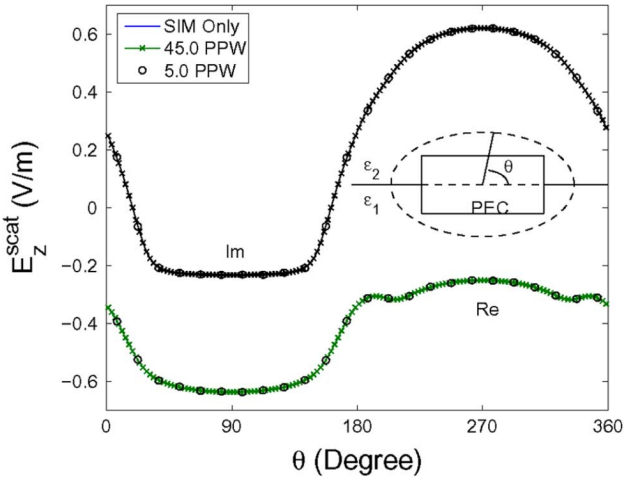

Fig. 6. Scattered field along the radiation boundary ($r = (0.2, 0.1)$ m) for a rectangular PEC object (12.5 cm × 5 cm) in a two-layer medium. $\mu_{r,2} = \epsilon_{r,2} = \mu_{r,1} = 1, \epsilon_{r,1} = 4, f = 300$ MHz.

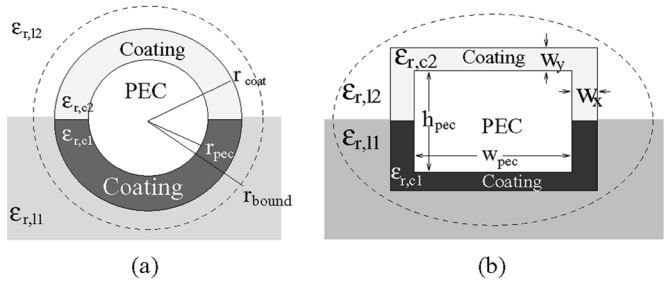

Fig. 7. Inhomogeneous scatterers. (a) Circular and (b) rectangular PEC cylinder surrounded with coating in a two-layer medium, $\epsilon_{r,l1} = 4, \epsilon_{r,l2} = 1$.

TABLE I
CIRCULAR COATING MODELS

	(a)	(b)	(c)	(d)
$\epsilon_{r,c1}$	16	9	4	4
$\epsilon_{r,c2}$	16	9	4	1

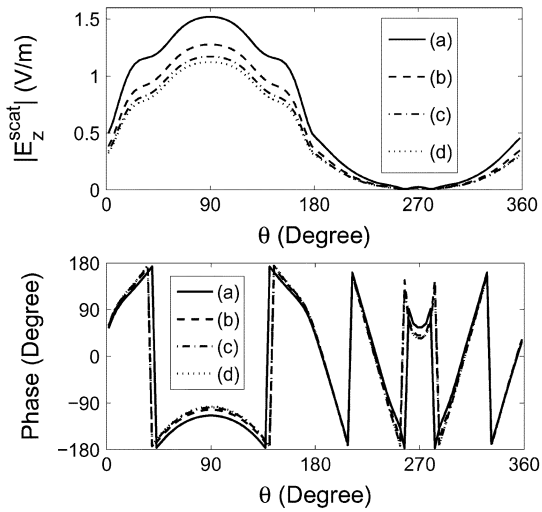

Fig. 8. Magnitude and phase of the scattered fields along the radiation boundary for a circular PEC object surrounded with coating, $r_{\text{bound}} = 0.6$ m, $r_{\text{coat}} = 0.55$ m, and $r_{\text{pec}} = 0.5$ m in a two-layer medium. $f = 300$ MHz.

C. Rectangular Cylinder/Elliptical Boundary

The circular PEC object presented in the previous example is then replaced by a rectangular PEC object (12.5 cm × 5 cm). In this case, an elliptical radiation boundary with major axis $a = 0.2$ m and minor axis $b = 0.1$ m is used. The number of triangular elements is 2670, and the number of FEM nodes is 1525. Fig. 5 shows the normalized magnitude of current induced on the object, the SIM/FEM result (5 PPWs) agrees very well with the MFIE solution [30]. Fig. 6 shows the scattered field along the radiation boundary obtained with the SIM/FEM method (5 and 45 PPWs), and SIM alone (10 PPWs). Again, an excellent agreement has been observed. The difference between the SIM/FEM results obtained by using 5 and 45 PPWs is less than 1%.

D. Circular Scatterer With Coating

The previous two examples show that the hybrid SIM/FEM works well for homogeneous objects. In this example, the scatterer, shown in Fig. 7(a), is an inhomogeneous scatterer. The frequency is 300 MHz, $r_{\text{bound}} = 0.6$ m, $r_{\text{coat}} = 0.55$ m, $r_{\text{pec}} = 0.5$ m, and $\epsilon_{r,l1} = 4, \epsilon_{r,l2} = 1$. The number of triangular elements is 2462, and the number of FEM nodes is 1437. In this example, we used four different sets of $(\epsilon_{r,c1}, \epsilon_{r,c2})$ values, which are given in Table I. Note that case (d) is the same as the example in Fig. 3. Fig. 8 shows the magnitude and phase of the scattered fields for the four different cases, respectively. The gradual change in the scattered field from (a) through (d) clearly depicts the effect of coating.

E. Rectangular Scatterer With Coating

Similarly, a rectangular PEC object used in Fig. 6 is coated with different materials, as shown in Fig. 7(b). Again, $f = 300$ MHz, $r_{\text{bound}} = (20, 10)$ cm for the elliptical outer boundary, $w_{\text{pec}} = 12.5$ cm, $h_{\text{pec}} = 5.0$ cm; $w_x = 1.0$ cm, $w_y = 1.5$ cm; $\epsilon_{r,l1} = 4$, and $\epsilon_{r,l2} = 1$. The center of the object is on the interface. The number of triangular elements is 3376, and the number of FEM nodes is 1878. Four different sets of $(\epsilon_{r,c1}, \epsilon_{r,c2}, \sigma_1, \sigma_2)$ values are used for the coating, which are given in Table II. Note that case (d) is the same as Fig. 6. Fig. 9 shows the magnitude and phase of the scattered fields for the four different cases, respectively. Similar to the previous

TABLE II
RECTANGULAR COATING MODELS

	(a)	(b)	(c)	(d)
$\epsilon_{r,c1}$	64	9	4	4
$\epsilon_{r,c2}$	64	9	4	1
σ_1 (S/m)	8	3	2	0
σ_2 (S/m)	8	3	2	0

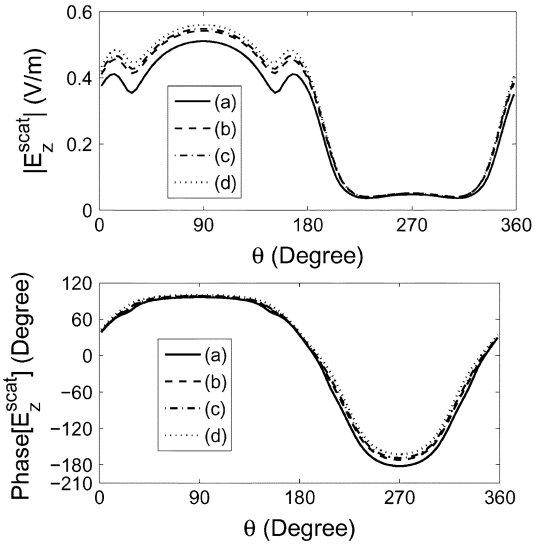

Fig. 9. Magnitude and phase of the scattered fields along the radiation boundary for a coated rectangular PEC object, $w_{\rm pec} = 12.5$ cm, $h_{\rm pec} = 5.0$ cm; $w_x = 1.0$ cm, $w_y = 1.5$ cm; $\epsilon_{r,l1} = 4$, and $\epsilon_{r,l2} = 1$ in a two-layer medium. $f = 300$ MHz.

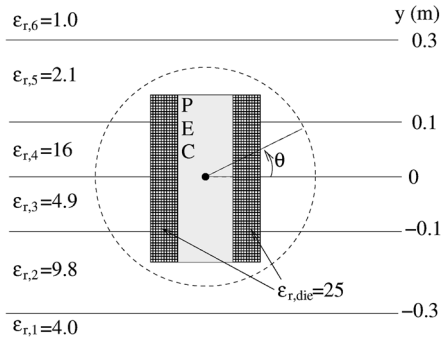

Fig. 10. Inhomogeneous scatterer residing in four layers of a six-layer background.

example, we can see the gradual change in the scattered field from (a) through (d).

F. Inhomogeneous Scatterer Residing in Four Layers

Finally, an inhomogeneous scatterer residing in four layers of a six-layer background, shown in Fig. 10, is analyzed. The inhomogeneous scatterer is centered at the origin, which is 30-cm long in the y-direction and 20-cm long in the x-direction. The middle part of the scatterer is a PEC with a width of 10 cm. There are dielectric coatings on the left and right sides of the scatterer with $\epsilon_{r,\rm die} = 25$ and 5 cm thick. The frequency of the incident field is 300 MHz. A circular boundary with a radius of

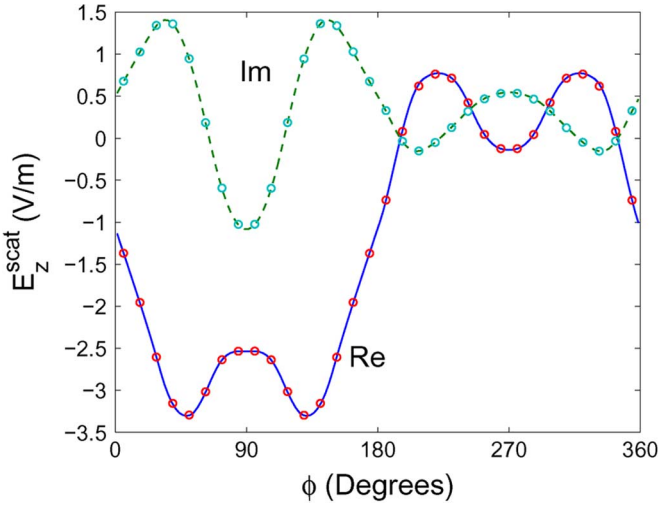

Fig. 11. Scattered field along the radiation boundary for an inhomogeneous scatterer residing in four layers.

20 cm is used as a radiation boundary, which has a circumference of $2\pi\lambda_{\rm die}$. The number of triangular elements is 4736, and the number of FEM nodes is 2558.

Fig. 11 shows the scattered field along the radiation boundary by using 5.7 PPWs (32 points) and 22.9 PPWs (144 points). A very good agreement has been observed between these two results.

As illustrated in this example, the hybrid FEM/SIM method is capable of solving scattering problems with inhomogeneous and composite structures residing in several layers of a layered medium.

V. CONCLUSION

In this paper, we have extended the SIM to the problems having a scatterer straddling several layers of a multilayered medium. Furthermore, we use the SIM as a novel RBC to truncate the computational domain of the FEM in a layered medium. Once we calculate the layered-medium Green's function for the RBC, we can use it several times for any type of object inside the artificial boundary. This hybrid SIM/FEM method is suitable for objects with arbitrary boundaries and structures. Numerical results show an overall second-order convergence because of using linear basis and testing functions in the FEM part. The number of points on the radiation boundary is only around 5 PPWs, thus giving substantial saving in memory and CPU time requirements. Applications are also demonstrated for inhomogeneous and composite structures.

REFERENCES

[1] B. Engquist and A. Majda, "Absorbing boundary conditions for the numerical simulation of waves," *Math. Comput.*, vol. 31, pp. 629–651, 1977.
[2] J. M. Jin and V. V. Liepa, "Application of hybrid finite element method to electromagnetic scattering from coated cylinders," *IEEE Trans. Antennas Propag.*, vol. 36, no. 1, pp. 50–54, Jan. 1988.
[3] J. M. Jin and V. V. Liepa, "A note on the hybrid finite element method for solving scattering problems," *IEEE Trans. Antennas Propag.*, vol. 36, no. 10, pp. 1486–1490, Oct. 1988.

[4] J. D. Collins, J. M. Jin, and J. L. Volakis, "A combined finite element—Boundary element formulation for solution of two-dimensional problems via CGFFT," *Electromagnetics*, vol. 10, no. 4, pp. 423–437, 1990.
[5] J. M. Jin, J. L. Volakis, and J. D. Collins, "A finite element—Boundary integral method for scattering and radiation by two- and three-dimensional structures," *IEEE Antennas Propag. Mag.*, vol. 33, no. 3, pp. 22–32, Jun. 1991.
[6] J. M. Jin and J. L. Volakis, "A hybrid finite element method for scattering and radiation by microstrip patch antennas and arrays residing in a cavity," *IEEE Trans. Antennas Propag.*, vol. 39, no. 11, pp. 1598–1604, Nov. 1991.
[7] J. P. Berenger, "A perfectly matched layer for the absorption of electromagnetic waves," *J. Comput. Phys.*, vol. 114, pp. 185–200, Oct. 1994.
[8] Z. S. Sachs, D. M. Kingsland, R. Lee, and J.-F. Lee, "Performance of an anisotropic artificial absorber for truncating finite element meshes," *IEEE Trans. Antennas Propag.*, vol. 43, no. 12, pp. 1460–1463, Dec. 1995.
[9] W. C. Chew and W. H. Weedon, "A 3-D perfectly matched medium from modified Maxwell's equations with stretched coordinates," *Microw. Opt. Technol. Lett.*, vol. 7, pp. 599–604, 1994.
[10] S. D. Gedney, "An anistropic perfectly matched layer—Absorbing medium for truncation of FDTD lattices," *IEEE Trans. Antennas Propag.*, vol. 44, no. 12, pp. 1630–1639, Dec. 1996.
[11] M. D. Deshpande, C. R. Cockrell, and C. J. Reddy, "Electromagnetic scattering analysis of arbitrarily shaped material cylinder by FEM-BEM method," NASA Langley Res. Center, Hampton, VA, NASA Tech. Rep., Jul. 1996.
[12] Q. H. Liu, "An FDTD algorithm with perfectly matched layers for conductive media," *Microw. Opt. Technol. Lett.*, vol. 14, no. 2, pp. 134–137, 1997.
[13] M. W. Ali, T. H. Hubing, and J. L. Drewniak, "A hybrid FEM/MoM technique for electromagnetic scattering and radiation from dielectric objects with attached wires," *IEEE Trans. Electromagn. Compat.*, vol. 39, no. 4, pp. 304–314, Nov. 1997.
[14] J. Jin, *The Finite Element Method in Electromagnetics*. New York: Wiley, 1993.
[15] J. L. Volakis, A. Chatterjee, and L. C. Kempel, *Finite Element Method for Electromagnetics*. Piscataway, NJ: IEEE Press, 1998.
[16] A. F. Peterson, A. L. Ray, and R. Mittra, *Computational Methods for Electromagnetics*. Piscataway, NJ: IEEE Press, 1998, p. 43.
[17] A. Musolino and M. Raugi, "A hybrid FEM/MOM formulation for nonlinear electromagnetic analysis," *IEEE Trans. Magn.*, vol. 34, no. 5, pp. 3292–3295, Sep. 1998.
[18] F. L. Teixeira and W. C. Chew, "A general approach to extend Berenger's absorbing boundary condition to anisotropic and dispersive media," *IEEE Trans. Antennas Propag.*, vol. 46, no. 9, pp. 1386–1387, Sep. 1998.
[19] J. A. Roden and S. D. Gedney, "Convolution PML (CPML): An efficient FDTD implementation of the CFS-PML for arbitrary media," *Microw. Opt. Technol. Lett.*, vol. 27, no. 5, pp. 334–339, 2000.
[20] G. X. Fan and Q. H. Liu, "A strongly well-posed PML in lossy media," *IEEE Antennas Wireless Propag. Lett.*, vol. 2, no. 7, pp. 97–100, 2003.
[21] A. Musolino, "Finite-element method/method of moments formulation for the analysis of current distribution in rail launchers," *IEEE Trans. Magn.*, vol. 41, no. 1, pp. 387–392, Jan. 2005.
[22] J. Liu and Q. H. Liu, "A spectral integral method (SIM) for periodic and nonperiodic structures," *IEEE Microw. Wireless Compon. Lett.*, vol. 14, no. 3, pp. 97–99, Mar. 2004.
[23] E. Simsek, J. Liu, and Q. H. Liu, "A spectral integral method (SIM) for layered media," *IEEE Trans. Antennas Propag.*, vol. 54, no. 6, pp. 1742–1749, Jun. 2006.
[24] J. Liu and Q. H. Liu, "A novel radiation boundary condition for finite-element method," *J. Comput. Phys.*, submitted for publication.
[25] K. A. Michalski and D. Zheng, "Electromagnetic scattering and radiation by surfaces of arbitrary shape in layered media: Part I: Theory," *IEEE Trans. Antennas Propag.*, vol. 38, no. 3, pp. 335–344, Mar. 1990.
[26] K. A. Michalski and J. R. Mosig, "Multilayered media Green's functions in integral equation formulations," *IEEE Trans. Antennas Propag.*, vol. 45, no. 3, pp. 508–519, Mar. 1997.
[27] W. C. Chew, *Waves and Fields in Inhomogeneous Media*. Piscataway, NJ: IEEE Press, 1995.
[28] E. Simsek, Q. H. Liu, and B. Wei, "Singularity subtraction for evaluation of Green's functions for multilayer media," *IEEE Trans. Microw. Theory Tech.*, vol. 54, no. 1, pp. 216–225, Jan. 2006.
[29] F. Q. Hu, "A spectral boundary integral equation method for the 2-D Helmholtz equation," *J. Comput. Phys.*, vol. 120, pp. 340–347, 1995.
[30] X.-B. Xu and C. M. Butler, "Scattering of TM excitation by coupled and partially buried cylinders at the interface between two media," *IEEE Trans. Antennas Propag.*, vol. AP-35, no. 5, pp. 529–538, May 1987.

Ergün Şimşek (S'01) received the B.S. degree in electrical engineering from Bilkent University, Ankara, Turkey, in 2001, the M.S. degree in electrical and computer engineering from the University of Massachusetts at Dartmouth, in 2003, and is currently working toward the Ph.D. degree at Duke University, Durham, NC.

Since 2003, he has been a Research Assistant with Duke University. His research interests include numerical methods and computational electromagnetics.

Jianguo Liu (S'05) received the B.S. degree in physics from Northeast Normal University, Changchun, China, in 1995, the M.E. degree in underwater acoustics engineering from Harbin Engineering University, Harbin, China, in 1998, and is currently working toward the Ph.D. degree at Duke University, Durham, NC.

From 1998 to 2003, he was with the Institute of Acoustics, Chinese Academy of Sciences. Since 2003, he has been a Research Assistant with Duke University. His research interests are computational acoustics, experimental underwater sound propagation, and computational electromagnetics.

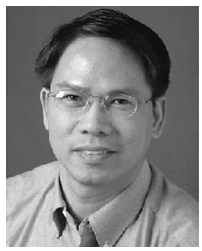

Qing Huo Liu (S'88–M'89–SM'94–F'05) received the Ph.D. degree in electrical engineering from the University of Illinois at Urbana-Champaign, in 1989.

From September 1986 to December 1988, he was with the Electromagnetics Laboratory, University of Illinois at Urbana-Champaign as a Research Assistant, and from January 1989 to February 1990, he was a Post-Doctoral Research Associate. From 1990 to 1995, he was a Research Scientist and Program Leader with Schlumberger-Doll Research, Ridgefield, CT. From 1996 to May 1999, he was an Associate Professor with New Mexico State University. Since June 1999, he has been with Duke University, Durham, NC, where he is currently a Professor of electrical and computer engineering. He has authored or coauthored over 300 papers in refereed journals and conference proceedings. He is an Associate Editor for *Radio Science*. His research interests include computational electromagnetics and acoustics, inverse problems, geophysical subsurface sensing, biomedical imaging, electronic packaging, and the simulation of photonic devices and nanodevices.

Dr. Liu is a Fellow of the Acoustical Society of America. He is a member of Phi Kappa Phi, and Tau Beta Pi. He is a full member of the U.S. National Committee, URSI Commissions B and F. He is an associate editor for the IEEE TRANSACTIONS ON GEOSCIENCE AND REMOTE SENSING, for which he also served as a guest editor for the "Special Issue on Computational Methods." He was the recipient of the 1996 Presidential Early Career Award for Scientists and Engineers (PECASE) presented by the White House, the 1996 Early Career Research Award presented by the Environmental Protection Agency, and the 1997 CAREER Award presented by the National Science Foundation (NSF).